AMERICAN SOCIETY FOR MICROBIOLOGY Journal of Virology®

PATHOGENESIS AND IMMUNITY

[^{18}F]-Fluorodeoxyglucose Uptake in Lymphoid Tissue Serves as a Predictor of Disease Outcome in the Nonhuman Primate Model of Monkeypox Virus Infection

Julie Dyall,[a] Reed F. Johnson,[b] Svetlana Chefer,[a] Christopher Leyson,[a] David Thomasson,[a] Jurgen Seidel,[a] Dan R. Ragland,[a] Russell Byrum,[a] Catherine Jett,[a*] Jennifer A. Cann,[a*] Marisa St. Claire,[a] Elaine Jagoda,[c] Richard C. Reba,[a,d] Dima Hammoud,[a,d] Joseph E. Blaney,[b,c*] Peter B. Jahrling[a,b]

Integrated Research Facility, National Institute of Allergy and Infectious Diseases, National Institutes of Health, Frederick, Maryland, USA[a]; Emerging Viral Pathogens Section, National Institute of Allergy and Infectious Diseases, National Institutes of Health, Frederick, Maryland, USA[b]; Molecular Imaging Program, National Cancer Institute, National Institutes of Health, Bethesda, Maryland, USA[c]; Center for Infectious Disease Imaging, Radiology and Imaging Sciences, Clinical Center, National Institutes of Health, Bethesda, Maryland, USA[d]

ABSTRACT Real-time bioimaging of infectious disease processes may aid countermeasure development and lead to an improved understanding of pathogenesis. However, few studies have identified biomarkers for monitoring infections using *in vivo* imaging. Previously, we demonstrated that positron emission tomography/computed tomography (PET/CT) imaging with [^{18}F]-fluorodeoxyglucose (FDG) can monitor monkeypox disease progression *in vivo* in nonhuman primates (NHPs). In this study, we investigated [^{18}F]-FDG-PET/CT imaging of immune processes in lymphoid tissues to identify patterns of inflammation in the monkepox NHP model and to determine the value of [^{18}F]-FDG-PET/CT as a biomarker for disease and treatment outcomes. Quantitative analysis of [^{18}F]-FDG-PET/CT images revealed differences between moribund and surviving animals at two sites vital to the immune response to viral infections, bone marrow and lymph nodes (LNs). Moribund NHPs demonstrated increased [^{18}F]-FDG uptake in bone marrow 4 days postinfection compared to surviving NHPs. In surviving, treated NHPs, increase in LN volume correlated with [^{18}F]-FDG uptake and peaked 10 days postinfection, while minimal lymphadenopathy and higher glycolytic activity were observed in moribund NHPs early in infection. Imaging data were supported by standard virology, pathology, and immunology findings. Even with the limited number of subjects, imaging was able to differentiate the difference between disease outcomes, warranting additional studies to demonstrate whether [^{18}F]-FDG-PET/CT can identify other, subtler effects. Visualizing altered metabolic activity at sites involved in the immune response by [^{18}F]-FDG-PET/CT imaging is a powerful tool for identifying key disease-specific time points and locations that are most relevant for pathogenesis and treatment.

IMPORTANCE Positron emission tomography and computed tomography (PET/CT) imaging is a universal tool in oncology and neuroscience. The application of this technology to infectious diseases is far less developed. We used PET/CT imaging with [^{18}F]-labeled fluorodeoxyglucose ([^{18}F]-FDG) in monkeys after monkeypox virus exposure to monitor the immune response in lymphoid tissues. In lymph nodes of surviving monkeys, changes in [^{18}F]-FDG uptake positively correlated with enlargement of the lymph nodes and peaked on day 10 postinfection. In contrast, the bone marrow and lymph nodes of nonsurvivors showed increased [^{18}F]-FDG uptake by day 4 postinfection with minimal lymph node enlargement, indicating that elevated

Received 31 May 2017 **Accepted** 14 July 2017

Accepted manuscript posted online 16 August 2017

Citation Dyall J, Johnson RF, Chefer S, Leyson C, Thomasson D, Seidel J, Ragland DR, Byrum R, Jett C, Cann JA, St. Claire M, Jagoda E, Reba RC, Hammoud D, Blaney JE, Jahrling PB. 2017. [^{18}F]-Fluorodeoxyglucose uptake in lymphoid tissue serves as a predictor of disease outcome in the nonhuman primate model of monkeypox virus infection. J Virol 91:e00897-17. https://doi.org/10.1128/JVI.00897-17.

Editor Grant McFadden, The Biodesign Institute, Arizona State University

Address correspondence to Julie Dyall, dyallj@niaid.nih.gov.

* Present address: Catherine Jett, Department of Genetics, Texas Biomedical Research Institute, San Antonio, Texas, USA; Jennifer A. Cann, MedImmune, LLC, Gaithersburg, Maryland, USA; Joseph E. Blaney, Division of Intramural Research, National Institute of Allergy and Infectious Diseases, National Institutes of Health, Bethesda, Maryland, USA.

cell metabolic activity early after infection is predictive of disease outcome. [^{18}F]-FDG-PET/CT imaging can provide real-time snapshots of metabolic activity changes in response to viral infections and identify key time points and locations most relevant for monitoring the development of pathogenesis and for potential treatment to be effective.

KEYWORDS virus, orthopoxvirus, monkeypox virus, PET/CT, cidofovir, nonhuman primate, imaging, virus

Although smallpox was officially declared eradicated (1), the development of therapeutic agents for smallpox has continued because of the potential threat of bioterrorism attacks using variola virus and the emergence of zoonotic poxviral infections such as monkeypox. Conducting large-scale human trials of smallpox antiviral agents presents significant challenges, as monkeypox occurs mostly in rural and remote areas of Central and Western Africa. Outside of Africa, monkeypox outbreaks are sporadic and affect a small number of patients. The "animal rule" permits the use of animal models of monkeypox or smallpox to link antiviral efficacy to clinical outcome in lieu of human clinical trials (2). Satisfying the animal rule for smallpox or monkeypox therapeutic agents constitutes a major challenge, since none of the animal models fully replicate human smallpox or monkeypox (3).

Biomarker measurements as surrogate indicators of normal or pathogenic processes have great value in efficacy and safety evaluations for novel therapeutic agents in *in vivo* animal models (4). Biomarkers, such as pox lesion counts and blood viral load, are measurements commonly used in orthopoxvirus animal models for countermeasure evaluation (5–7). However, virus dissemination in organs is difficult to determine by standard virological techniques and can be estimated only by quantifying virus loads in small tissue samples from serial sacrifice studies, which require large numbers of animals.

Imaging modalities, such as positron emission tomography/computed tomography (PET/CT), may support preclinical testing, reduce the number of required study subjects, and provide additional data that cannot be gained from conventional testing methods. Previously, we demonstrated that [^{18}F]-labeled fluorodeoxyglucose ([^{18}F]-FDG)-PET/CT imaging can be used to monitor monkeypox disease progression in nonhuman primates (NHPs) in real time (8, 9). [^{18}F]-FDG-PET imaging has been used for elucidating the host immune response and patterns of inflammation of various infectious diseases, such as AIDS, tuberculosis, and influenza (10–14). However, few studies have been performed to identify biomarkers for monitoring infections using *in vivo* imaging and to determine the value of biomarkers as reliable endpoint criteria in preclinical studies of treatments (15, 16).

In this study, we investigated [^{18}F]-FDG-PET/CT imaging of immune processes in lymphoid tissues to predict survival/lethality of monkeypox. For proof of concept, cidofovir (CDV), a known antiviral for poxvirus infections, was used to determine the predictive value of potential biomarkers in treated versus untreated animals infected with monkeypox.

RESULTS

Standard characterization of monkeypox in nonhuman primates. The experimental design of this monkeypox virus (MPXV) intravenous (IV) challenge study and treatment with CDV is shown in Table 1. Clinical manifestations of the untreated and treated groups are summarized in Table 2. All three CDV-treated NHPs (CDV-1 to CDV-3) survived. Two NHPs in the untreated control group met clinical endpoint criteria (UNTR-1, UNTR-3), and one survived (UNTR-2). All animals developed fever irrespective of treatment or survival status on days 1 and 2 postinfection (p.i.). The main differences in clinical signs between CDV-treated and untreated animals were skin lesion development and viremia (Table 2). The mean day for the appearance of lesions was 6.3 in survivors, while the moribund subjects did not develop any lesions before reaching

TABLE 1 Study endpoint and schedule for PET and CT imaging

NHP[a] no.	Study endpoint	Baseline scans (day)	Postinfection scans (day)[b]
CDV-1	Survived	−20, −12, −5	1, 3, 8, 10, 16, 22
CDV-2	Survived	−20, −12, −5	1, 3, 8, 10, 16, 22
CDV-3	Survived	−20, −12, −5	1, 3, 8, 10, 16, 22
UNTR-1	Became moribund (day 7)	−19, −11, −4	2, 4, (7)[c]
UNTR-2	Survived	−19, −11, −4	2, 4, 8, 10, 16, 22
UNTR-3	Became moribund (day 7)	−19, −11, −4	2, 4, 7[d]

[a]Abbreviations: CDV, cidofovir; NHP, nonhuman primate; UNTR, untreated.
[b]Scans were performed on the indicated days until day 22 or until the NHP became moribund.
[c]UNTR-1 was not imaged on day of endpoint.
[d]UNTR-3 was imaged on day of endpoint.

clinical endpoint (day 7 p.i.). Treatment with CDV delayed lesion appearance and peak by 2 days and reduced skin lesion numbers by 5-to 10-fold compared to that for the untreated survivor. Similar to a previous study, CDV treatment delayed viremia by 6 days and reduced peak virus load as measured by quantitative PCR. CDV treatment reduced viral load by 2.4 $\log_{10}$ in comparison to that observed in untreated animals (17). Antibody titers were in the same range (1:500 to 1:600) for the three treated NHPs and the untreated survivor and peaked on day 16 p.i. (Table 2). Antibody titers were not detected in two moribund subjects.

Moribund subjects had significantly higher [18F]-FDG uptake in bone marrow. Fused [18F]-FDG-PET and CT images were used to monitor [18F]-FDG uptake in bone marrow (BM) of the manubrium pre- and postinfection with MPXV. Three preexposure imaging sessions were performed per NHP to determine baseline values for [18F]-FDG uptake. Healthy NHPs demonstrated moderate [18F]-FDG uptake over a period of 3 weeks before exposure (mean standardized uptake value [SUV_{mean}] = 3.02 ± 0.88) (Fig. 1A). In infected NHPs, an increase in [18F]-FDG uptake in BM above baseline was observed on day 1 or 2 p.i. (Fig. 1B). On day 3 or 4 pi, the two NHPs that would meet study endpoint criteria (UNTR-1 and UNTR-3) had additional strong elevations in [18F]-FDG-BM uptake that were not noted in the four surviving NHPs. In the surviving NHPs, [18F]-FDG uptake gradually returned to baseline values by day 21 p.i. (SUV_{mean} = 3.76 ± 0.74) (Fig. 1A) irrespective of treatment. An exploratory 2-way analysis of variance (ANOVA) of data up to day 3 or 4 p.i. showed that [18F]-FDG uptake in BM was affected by time and survival status (Fig. 1B). Moribund NHPs demonstrated significantly higher uptake ($P < 0.01$) of [18F]-FDG in BM ($SUV_{mean} = 9.33 \pm 2.29$; $n = 2$) than surviving NHPs (SUV = 5.63 ± 0.97; $n = 4$; Fig. 1B and C).

A previous study with cancer patients reported the correlation between [18F]-FDG uptake in BM and white blood cell (WBC) counts (18). To investigate correlations between BM glycolytic activity and various hematological parameters, blood samples were collected on the same days as imaging data were acquired. BM [18F]-FDG uptake

TABLE 2 Characteristics of monkeypox disease progression

Clinical parameter	Cidofovir-treated group	Untreated group
No. of survivors/total in group	3/3	1/3
Day of death	All survived	7 (n = 2)
Mean day of lesion onset	6.3	4 (n = 1; survivor)
Mean day of peak lesion counts	12	10 (n = 1; survivor)
Range of peak lesion counts	122–280	1,082 (n = 1; survivor)
Mean day of viremia appearance	8	2 (n = 3)
Mean day of peak viremia	10	7.5 (n = 2)[a]
Mean peak viremia ($\log_{10}$ gene copies/ml)	3.3	7.96[a]
Mean day of fever onset	1	2
Range of peak temp (°C)	40–40.7	39.2–39.5
Mean day of peak antibody response	16	16 (n = 1; survivor)
Mean peak antibody titer (serum dilution)[b]	500	500 (n = 1; survivor)

[a]Average for 2 NHPs (1 of 3 NHPs became moribund on day 6 of 7; no sample was taken).
[b]Titers were determined as the inverse of the serum dilution with 50% plaque reduction.

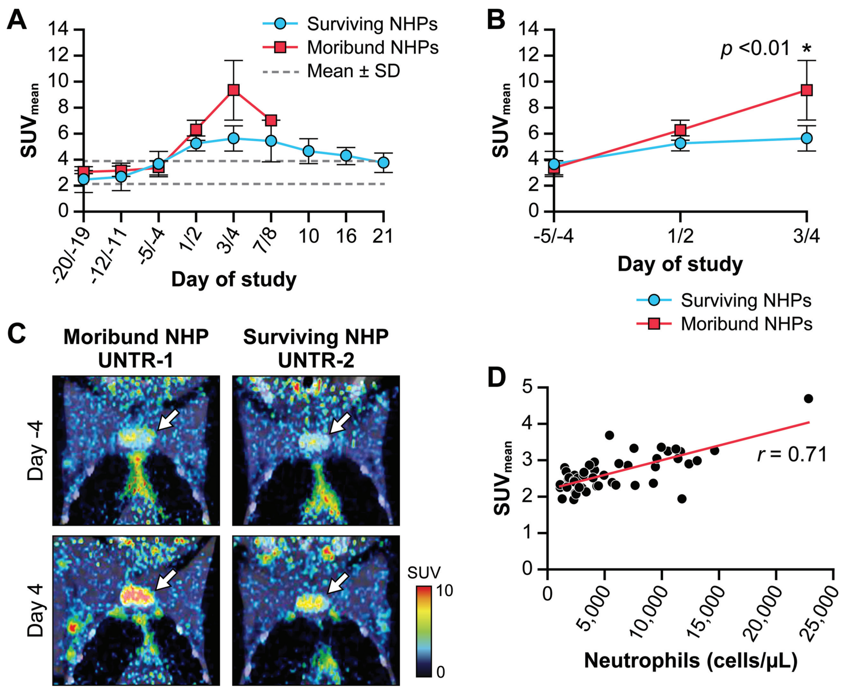

FIG 1 Longitudinal changes in [18F]-FDG uptake in BM induced by monkeypox in NHPs. (A) [18F]-FDG uptake in the BM in moribund and surviving groups on different days pre- and postinfection. Dotted lines represent the mean ± standard deviation (SD) of the 18 (6 NHPs × 3 scans) baseline SUV_{mean} for the BM obtained prior to virus exposure. (B) Changes in SUV_{mean} in the BM during the early stage of MPXV infection. Each data point represents an average value for moribund (red; $n = 2$) and surviving (blue; $n = 4$) groups (mean ± SD). Two-way ANOVA for repeated measures determined a statistically significant difference, $P < 0.01$, in [18F]-FDG BM uptake between moribund and surviving groups on day 3 or 4 p.i. (*). (C) Representative [18F]-FDG-PET images of the upper chest fused with corresponding CT images of one moribund NHP (UNTR-1) and one untreated survivor (UNTR-2) on days −4 preexposure and +4 p.i. VOIs (not shown) were drawn around the manubrium marked by white arrows on the images in the coronal view. (D) Correlation between [18F]-FDG uptake in BM and neutrophils in the blood. Each data point represents one scan on one of six animals on 1 of 18 imaging days. The statistical significance (r) of the correlation was determined using the Pearson product moment correlation coefficient exposure.

correlated with the WBC counts throughout the course of disease ($r = 0.52$; $P = 0.0002$) but not with red blood cell (RBC) counts (Table 3). Throughout progression/regression of MPXV infection, [18F]-FDG uptake by BM highly correlated with the neutrophil counts ($P < 0.0001$) (Fig. 1D).

Monkeypox-induced [18F]-FDG uptake and lymphadenopathy in lymph nodes. [18F]-FDG uptake was monitored in axillary and inguinal lymph nodes (LNs) pre- and postinfection with MPXV. Three preinfection imaging sessions were performed per NHP to determine baseline values for [18F]-FDG uptake and the normal LN volume. Analysis of fused PET and CT images demonstrated that MPXV infection induced an increase in [18F]-FDG uptake in LNs and lymphadenopathy in all six NHPs, albeit to various degrees (Fig. 2). Exploratory 2-way ANOVA of [18F]-FDG uptake showed significant differences between moribund and surviving subjects. In CDV-treated survivors, [18F]-FDG uptake in LNs gradually increased 4- to 9-fold, and LN volumes increased 3- to 4-fold and

TABLE 3 Correlation coefficient between bone marrow SUVs and blood cell types

Blood cell type	Correlation coefficient[a] (r)
Neutrophil	0.71****
Monocyte	0.56****
White blood cell	0.52***
Lymphocyte	0.15
Red blood cell	0.14

[a]***, $P = 0.0002$; ****, $P < 0.0001$.

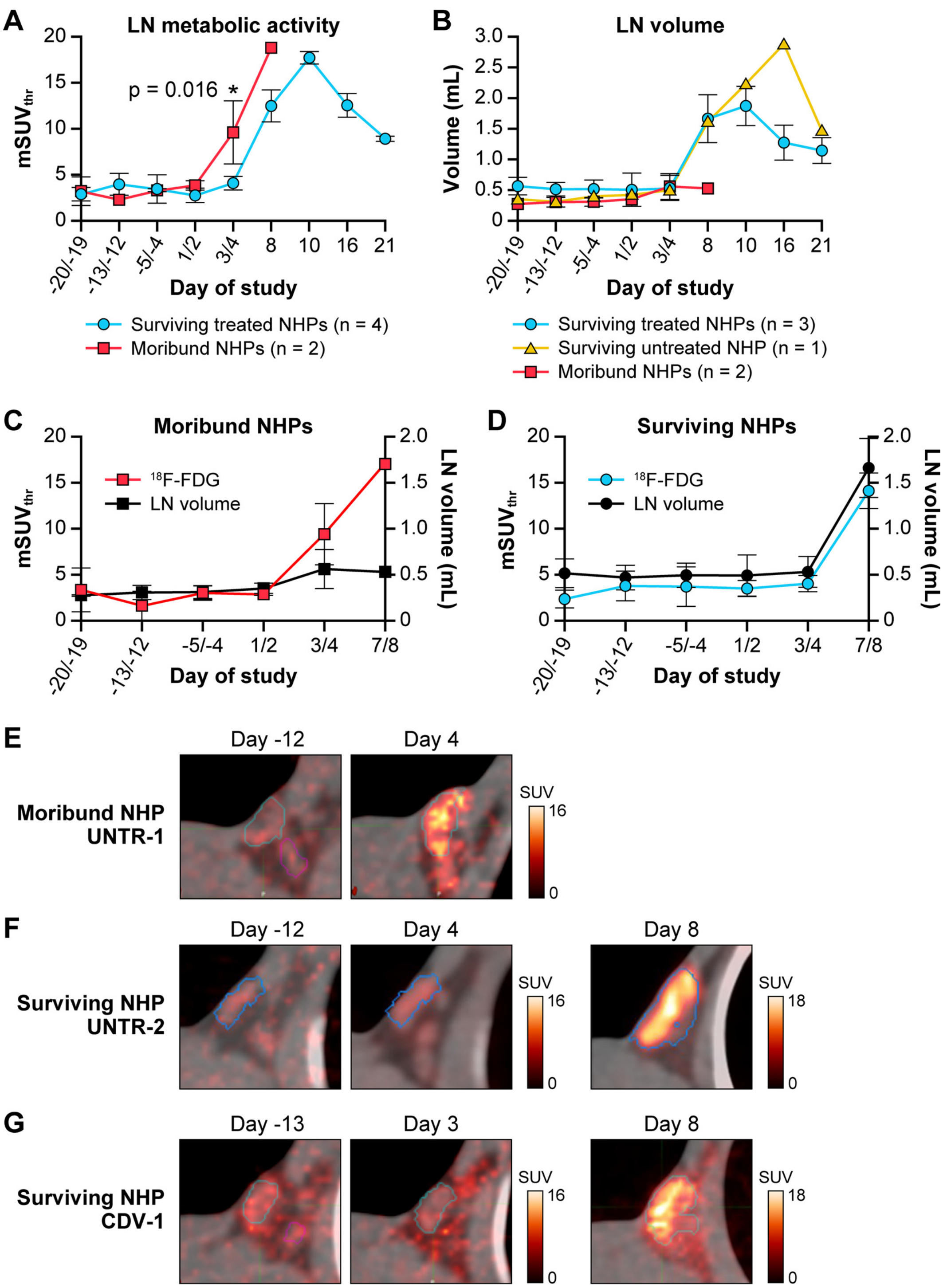

FIG 2 Longitudinal changes in [18F]-FDG uptake in LNs induced by monkeypox. (A) Changes in [18F]-FDG uptake were measured by the standardized uptake value ($mSUV_{thr}$) over time in the right axillary LN in NHPs that survived ($n = 4$) or became moribund ($n = 2$). Two-way ANOVA for repeated measures determined a statistically significant difference ($P = 0.016$) between moribund and surviving groups on day 3 or 4 p.i. (*). (B) Changes in the volume of the right axillary LN over time were measured by CT images in moribund and CDV-treated and untreated surviving NHPs. (C) Longitudinal changes in LN glycolytic activity ($mSUV_{thr}$) and volume (ml) in moribund ($n = 2$) NHPs (mean ± SD). (D) Longitudinal changes in LN glycolytic activity ($mSUV_{thr}$) and volume (ml) in surviving groups ($n = 4$; mean ± SD). (E to G) Representative [18F]-FDG-PET images of axillary LNs fused with corresponding CT images of one moribund NHP (UNTR-1) (E), one untreated survivor (UNTR-2) (F), and one treated survivor (CDV-1) (G) at the indicated days pre- or postinoculation. Abbreviations: CDV, cidofovir; [18F]-FDG, [18F]-fluorodeoxyglucose; LN, lymph node; $mSUV_{thr}$, modified $SUV_{threshold}$; NHP, nonhuman primate; p.i., postinfection; UNTR, untreated; VOI, volume of interest.

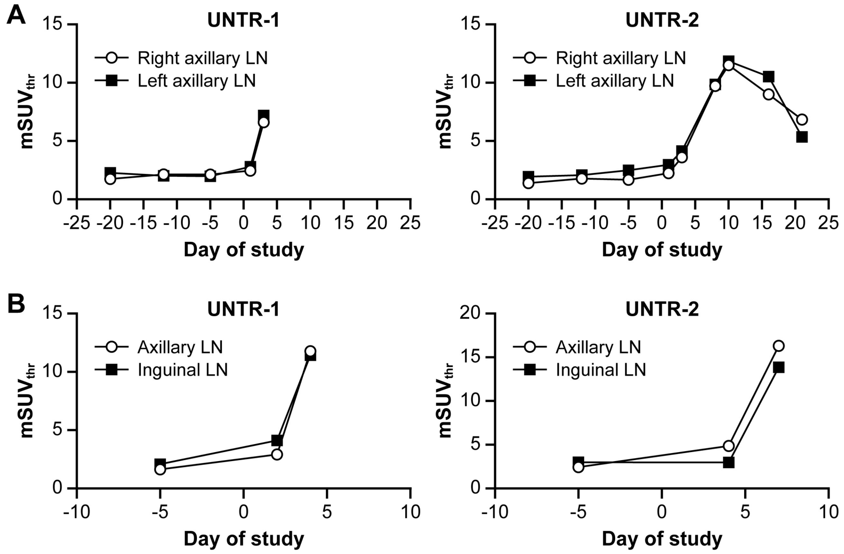

FIG 3 Changes in [^{18}F]-FDG uptake during MPXV infection of NHPs in LNs at different locations. (A) [^{18}F]-FDG uptake in the right- and left-side axillary LNs in one moribund NHP (UNTR-1) and one survivor (UNTR-2). (B) [^{18}F]-FDG uptake in the axillary and inguinal LNs on select days in one moribund NHP (UNTR-1) and one survivor (UNTR-2). Abbreviations: [^{18}F]-FDG, [^{18}F]-fluorodeoxyglucose; LN, lymph node; MPXV, monkeypox virus; mSUV$_{thr}$, modified SUV$_{threshold}$; NHP, nonhuman primate; UNTR, untreated.

peaked on day 10 p.i. (Fig. 2A and B). In the untreated survivor (UNTR-2), the [^{18}F]-FDG uptake pattern was similar to that for the CDV-treated NHPs, with a peak on day 10 p.i. (7-fold increase). However, the duration of lymphadenopathy in the UNTR-2 survivor was longer and more pronounced (up to 8-fold enlargement on day 16 p.i.) than in treated survivors (Fig. 2B).

In contrast, [^{18}F]-FDG uptake values in the LNs in the moribund NHPs (UNTR-1, UNTR-3) at an early stage of infection (day 3 or 4 p.i.) were significantly higher than those observed in surviving NHPs ($P = 0.016$) (Fig. 2A) (8). The increase in LN volume in moribund NHPs was minimal (less than 2-fold) and did not increase in relation to the [^{18}F]-FDG uptake activity in the LNs (Fig. 2B and C). Survivors did not show increase in [^{18}F]-FDG uptake until day 8 p.i. (Fig. 2A), and in these animals, lymphadenopathy paralleled the changes in glycolytic activity (Fig. 2D). The high [^{18}F]-FDG uptake on day 4 p.i. in the moribund untreated NHP (UNTR-1) was not detected in the untreated surviving NHP (UNTR-2) that was scanned on the same day (Fig. 2E and F). In treated and untreated surviving NHPs, similar patterns of changes in [^{18}F]-FDG uptake in the LNs were observed irrespective of the timing of the scans (Fig. 2F and G).

CT-guided tracking of monkeypox-induced lymphadenopathy and biopsies of LNs. The [^{18}F]-FDG uptake pattern for the LNs in axillary and inguinal areas followed the same trend during MPXV infection irrespective of LN location (left/right, axillary/inguinal) (Fig. 3A and 3B). Neighboring LNs within a cluster showed an overall comparable pattern of [^{18}F]-FDG uptake and lymphadenopathy, although the smaller LNs usually responded less strongly to viral infection. Through careful alignment of CT images on different days, lymphadenopathy was tracked, and individual LNs were surgically removed on day 9 p.i. (Fig. 4). By comparison of CT images acquired prior to (day 8 p.i.) and after (day 10 p.i.) biopsy, inguinal LNs removed for histological analysis were identified (Fig. 4A and B). The volume of LNs was determined by measuring their long and short axes in the axial plane of the slice in which those measurements appeared to be maximal in the whole node. The empirical LN volume determined following biopsy correlated well with the volume calculated from CT images (Fig. 4C and D). Surgical removal of an inguinal LN did not significantly alter the overall response of the remaining LNs.

Correlation of imaging data with histopathology and flow cytometry from LNs and peripheral blood mononuclear cells (PBMCs). We compared [^{18}F]-FDG uptake in

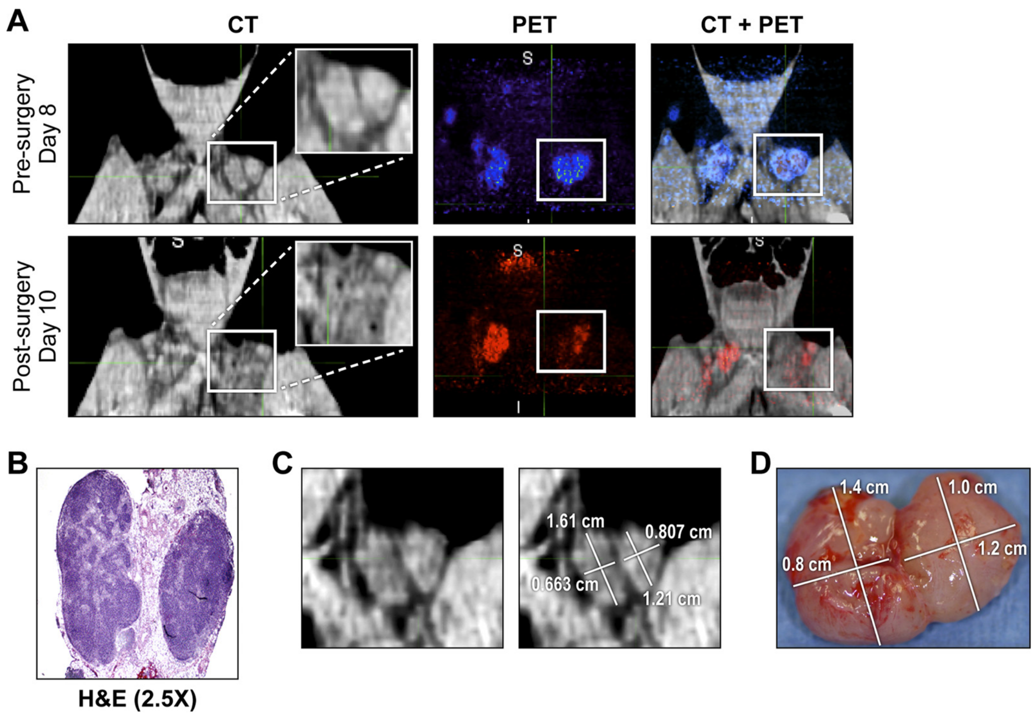

FIG 4 Tracking removal of inguinal LNs by PET/CT imaging. (A) CT, PET, and fused PET/CT images of the inguinal LN area in the untreated survivor (UNTR-2) acquired on days 8 and 10 p.i., before and after LN biopsy (day 9 p.i.), respectively. On the CT image, a white box marks the left-side inguinal LNs with an inset image of the magnified LN area. On day 8 or 10 p.i., the PET signal within the inguinal LN area was color-coded blue or red, respectively. (B) H&E staining of day-9-p.i.-biopsied LNs. (C) CT image of the two left-side LNs acquired on day 8 p.i. The sizes of the two LNs were determined using MIM5 software. (D) The actual sizes of the LNs were determined after removal on day 9 p.i. Abbreviations: H&E, hematoxylin & eosin; LN, lymph node; p.i., postinfection; UNTR, untreated.

axillary LNs (Fig. 5A and B) to histopathological and immunological changes in inguinal LN tissues. Results from immunohistochemical analysis with an antibody against Ki-67 identified proliferating cells in LNs from surviving CDV-treated (Fig. 5C) and untreated moribund (Fig. 5D) NHPs. T and B cells were identified with antibodies against CD4, CD8, or CD20 and were in the expected anatomical locations (data not shown) for these cell types. On day −19 preexposure (Fig. 5A and B), LN biopsy samples from both survivors and nonsurviving subjects demonstrated limited proliferation of B and T cells in cortical follicles and the paracortex, respectively, and minimal numbers of cells traversing the subcapsular sinuses (Fig. 5C and D). When [18F]-FDG uptake in survivors was high (day 9 p.i.) (Fig. 5A), increased numbers of histiocytes and proliferating B cells (verified by costaining with CD20 antibody; data not shown) in the subcapsular sinus and increased T-cell proliferation in the paracortex were observed (Fig. 5C). Lymphoid depletion with limited concurrent lymphocyte proliferation and edema was a prominent feature in the LNs of untreated nonsurvivors on day 7 p.i. (Fig. 5D). Sinus histiocytosis with large proliferating B cells was also detected in nonsurvivors, but was not as strong as in surviving animals. By day 22 p.i., recovering animals had normal LN architecture with strong follicular B-cell hyperplasia (Fig. 5C). Overall, the distinguishing characteristic of LNs among survivors at day 9 p.i. was uniform proliferation of T cells and B cells and increased sinus histiocytosis. By comparison, concurrent depletion of B cells and histiocytes and limited proliferation of lymphocytes in LNs were noted in both subjects that met endpoint criteria at day 7 p.i.

Flow cytometry of lymph nodes and blood supports the immunohistochemical findings. Ki-67 immunostaining of lymphocytes isolated from inguinal LN biopsies of surviving NHPs on day 9 p.i. confirmed the increase in proliferation of lymphocytes (e.g., $CD4^+$, $CD8^+$, and B cells) (Fig. 6A). The increase in Ki-67-positive cells in LNs was mirrored in the PBMC population with a small increase in proliferating $CD4^+$ and $CD8^+$

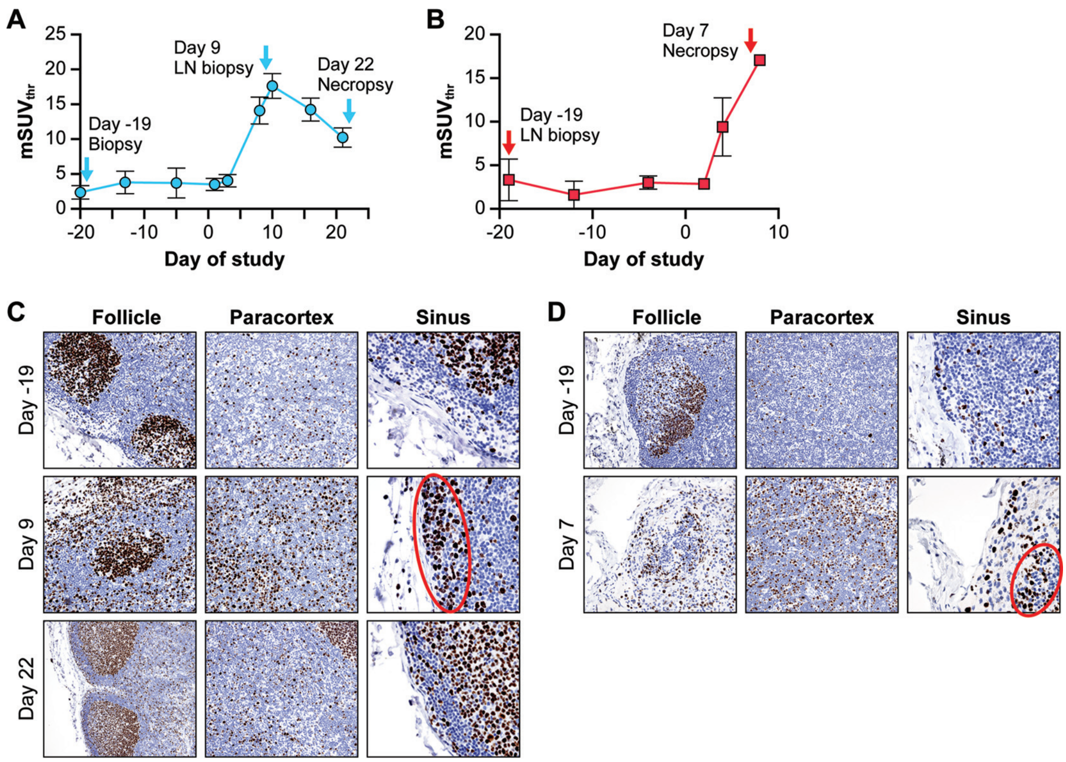

FIG 5 LN tissue characterization by immunohistochemistry and PET/CT imaging. (A) Changes in [^{18}F]-FDG uptake as measured by mSUV$_{thr}$ in axillary LNs of surviving NHPs. (B) Changes in [^{18}F]-FDG uptake measured via mSUV$_{thr}$ in axillary LNs of moribund NHPs. (C) Ki-67 staining of inguinal LN tissues from a surviving NHP (CDV-1) collected on day −19 preexposure and days 9 and 22 p.i. Areas of follicle, paracortex, and subcapsular sinus were scored for Ki-67-positive cells. The red oval shows Ki-67-positive proliferating B cells in the sinus. (D) Ki-67 staining of inguinal LN tissues from a moribund NHP (UNTR-1) collected on day −19 preexposure and day 7 p.i.at necropsy. Areas of follicle, paracortex, and subcapsular sinus were scored for Ki-67 and CD4, CD8, or CD20 (data not shown). The red oval shows Ki-67-positive proliferating B cells in the sinus. Abbreviations: CDV, cidofovir; [^{18}F]-FDG, [^{18}F]-fluorodeoxyglucose; LN, lymph node; mSUV$_{thr}$, modified SUV$_{threshold}$; NHP, nonhuman primate; p.i., postinfection; UNTR, untreated.

cells (9 to 12%) on day 8 p.i. in surviving animals (Fig. 6B and C). Only UNTR-2 demonstrated strong B-cell proliferation (approximately 40% of cells were Ki-67-positive on day 8 p.i.) that lasted into the recovery period (Fig. 6D). The increase in proliferating B cells could account for the greater LN volume in the UNTR-2 survivor than that observed in the CDV-treated NHPs (Fig. 2B).

DISCUSSION

[^{18}F]-FDG-PET/CT sequentially monitored progression of the immune response in BM and LNs after MPXV infection of rhesus macaques. Relatively little is known about the pathological significance of changes in [^{18}F]-FDG activity in BM during viral infections. Similar to that in healthy human subjects (18, 19), the baseline BM [^{18}F]-FDG uptake in healthy animals was moderate, and SUVs for glycolytic activity were reproducible for the same subject during the 3 weeks preexposure. On day 4 p.i., only the two animals that would eventually meet moribund endpoint criteria demonstrated a substantial increase in [^{18}F]-FDG uptake. Increased BM [^{18}F]-FDG uptake has been directly correlated with neutrophil mobilization in cancer patients (18, 19). Similarly, our results demonstrated a positive correlation between increased [^{18}F]-FDG uptake values in the BM and increased blood concentrations of neutrophils and monocytes in all NHPs. Thus, neutrophils and monocytes and/or other cells of the myeloid lineage are most likely responsible for the [^{18}F]-FDG uptake in the BM. The high BM [^{18}F]-FDG uptake in subjects that would become moribund may reflect a burst of proliferation associated with the strong cytokine responses induced in MPXV-infected NHPs (20), which is supported by results of an immunological substudy indicating that monocytes

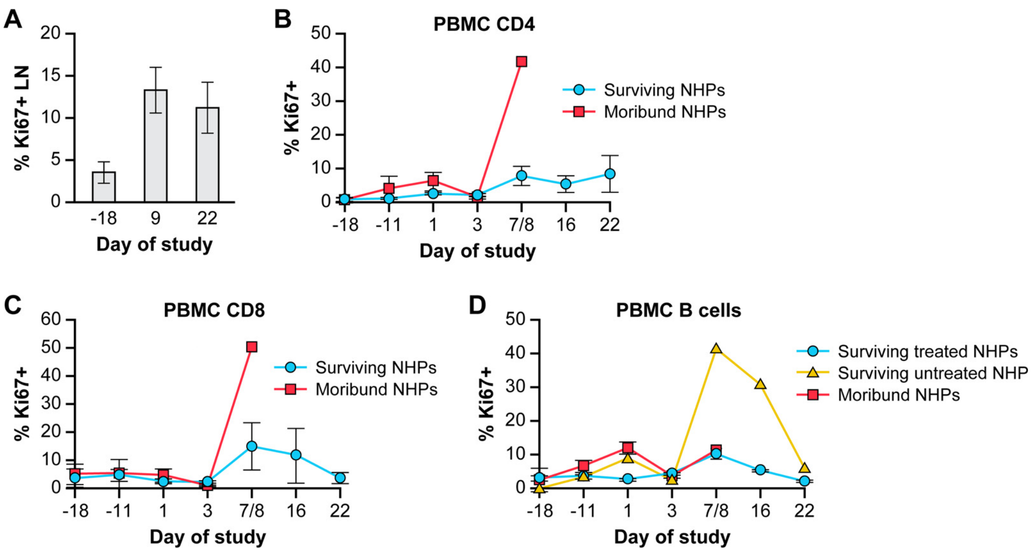

FIG 6 Proliferation of lymphocytes in LNs and PBMCs as measured by flow cytometry. (A) Ki-67 immunostaining of lymphocytes isolated from LNs of healthy animals on day −18 preexposure ($n = 2$) and from LNs of surviving animals ($n = 4$) on days 9 and 22 p.i. (B to D) Ki-67 immunostaining of CD4$^+$ T cells (B), CD8$^+$ T cells (C), and CD20$^+$ B cells (D) in PBMCs in treated and untreated survivors versus moribund NHPs. Abbreviations: LN, lymph node; NHP, nonhuman primate; PBMCs, peripheral blood mononuclear cells; p.i., postinfection.

are infected during the early stages of disease in moribund but not surviving NHPs (21). Importantly, this resulted in a significantly larger increase in the BM [^{18}F]-FDG signal (3-fold increase from baseline) in moribund NHPs than that observed in surviving NHPs (1.7-fold increase from baseline).

MPXV infection in NHPs and humans is characterized by marked lymphadenopathy (22). Lymphadenopathy is often considered an indication of functional activation, manifested by accumulation of activated macrophages and/or neutrophils and/or proliferation of T and B cells. However, lymphadenopathy can also be an indication of a pathological process within the lymph node. LN functional activation can be visualized by increased [^{18}F]-FDG uptake in these cells through PET imaging. Indeed, all NHPs treated with CDV showed a gradual elevation in LN volume that correlated with an increase in [^{18}F]-FDG uptake that peaked on day 10 p.i. and returned slowly to baseline during the recovery phase. Immunohistology of LN biopsies from day 9 p.i. detected histiocytosis and a mixed population of proliferating lymphocytes in the LN sinuses coinciding with high [^{18}F]-FDG uptake. Little or no edema or lymphoid depletion was observed. Instead, T- and B-cell LN proliferation (in the medulla and germinal centers, respectively) marked the beginning of a robust immune response that would be expected from subjects that recover from monkeypox disease.

However, in the two untreated moribund NHPs, [^{18}F]-FDG uptake in LNs did not correlate with LN volume. High [^{18}F]-FDG uptake was detected as early as day 4 p.i. when lymphadenopathy was minimal. Detailed statistical analysis was performed and reported previously (8). On day 7 p.i., necropsied LN tissues from moribund NHPs had high levels of edema and lymphoid necrosis and depletion. An earlier study had shown that monocytes in moribund subjects were positive for poxvirus antigen as early as 2 days p.i., while survivors did not show any antigen at all, indicating that infection of monocytes may play a role in pathogenesis (21). Based on the data from moribund subjects, one can hypothesize that monocytes become infected with MPXV early on, migrate to LNs, and induce a strong but short-lived burst of lymphocyte proliferation prior to extensive necrosis and depletion of lymphoid cells. Importantly, the high [^{18}F]-FDG uptake on day 4 p.i. was observed only in the two subjects that would become moribund and occurred without significant lymphadenopathy. The small number of subjects warrants additional studies to confirm these observations and investigate whether other, more subtle effects (e.g., treatment effects) than differentiating between disease outcomes can be demonstrated from an application of [^{18}F]-FDG-PET. Additional testing, such as autoradiography of LN tissues and [^{18}F]-FDG uptake assays on isolated LN cells, could confirm which cell subsets are ultimately responsible for [^{18}F]-FDG uptake at key time points in MPXV infection in moribund subjects versus survivors.

The [^{18}F]-FDG uptake patterns in both BM and LNs were similar in all four survivors irrespective of CDV treatment. Interestingly, the large reduction in virus replication in CDV-treated animals versus the higher viremia seen in the untreated survivor did not seem to affect the pattern of [^{18}F]-FDG uptake in lymphoid tissues. In contrast, lymphadenopathy in the untreated survivor, as monitored by CT, was more intense, lasted longer than in CDV-treated animals, and coincided with edema on day 9 p.i. and a strong B-cell response (PBMCs) on days 7 to 16 p.i. Therefore, treatment with CDV may reduce the viral burden and ameliorate lymphadenopathy by reducing edema and biasing the immune response toward recovery in the absence of the strong B-cell response seen in the untreated survivor.

The results of this study suggest that the early [^{18}F]-FDG uptake patterns of primary and secondary lymphoid tissues are crucial to acute viral pathogenesis and, as such, may have predictive value for disease outcome. The main differences in [^{18}F]-FDG patterns in BM and LNs were observed in surviving versus moribund subjects, and these differences could be exploited for development of imaging biomarkers to support preclinical studies of antipoxviral countermeasures. Larger animal numbers are required to confirm that the observed [^{18}F]-FDG uptake patterns in LN and BM have predictive value for determining the outcome of disease. The data presented here will assist in power analysis to determine the number of animals needed for the design of future studies. This pilot study identified key time points that warrant additional experiments, with biopsies taken at the same time points as imaging scans. The changes in [^{18}F]-FDG uptake after MPXV infection most likely represent a sum of processes with varied contributions from each process, depending on the infection stage. These processes might include a host immune response to the infection at early disease stages and pathological and pathophysiological changes at later disease stages. The most appropriate way to identify the specific mechanisms of these contributions is to investigate the correlations between the results of *in vitro* tissue evaluation and SUVs on the same day postinfection. Molecular processes could then be investigated in greater detail to understand which cell types contribute to the changes in [^{18}F]-FDG uptake. In addition, FDG/PET imaging can be combined with kinetic modeling methods for detecting small changes in cell metabolic activity with high sensitivity (influx rate constant K_i) (23) and provide another physiological parameter, tissue perfusion rate constant (K1), for evaluation by [^{18}F]-FDG/PET.

[^{18}F]-FDG-PET/CT application can be extended to any viral infection model, and [^{18}F]-FDG is commercially available. The method is well established and can support initial pathogenesis studies for developing models of novel emerging infectious diseases. The tools of immunology and pathology are essential for dissecting the immune response at a cellular or molecular level. However, [^{18}F]-FDG-PET/CT imaging can augment these methods to provide real-time snapshots of metabolic and pathological processes during viral infections to identify the key disease-specific time points and locations that are most relevant for treatment to be effective.

MATERIALS AND METHODS

Virus. Monkeypox virus (MPXV) Zaire 79 strain (V-79-I-005) was propagated in Vero E6 cells (CRL-1586; ATCC, Manassas, VA) at a multiplicity of infection (MOI) of 0.1 for 7 days. To prepare inoculum, Vero E6 cells were disrupted with a VCX-750 ultrasonic processor (Sonics, Newton, CT) for 120 s at 40% power on ice followed by centrifugation (500 $\times$ g, 10 min, 4°C).

Intravenous exposure of nonhuman primates. NHPs were screened to be seronegative for simian retrovirus, simian T cell leukemia, simian immunodeficiency virus, vaccinia virus, cowpox virus, and MPXV. Six male rhesus macaques (3 to 4 kg) were housed in biosafety level 3 containment and exposed by the IV route with 5 $\times$ 10^7 PFU of MPXV as described previously (20).

Ethics statement. Animals were housed in a facility accredited by the Association for Assessment and Accreditation of Laboratory Animal Care International. All experimental procedures were approved by the National Institute of Allergy and Infectious Diseases, Division of Clinical Research, Animal Care and Use Committee (protocol number OSD27E) and were in compliance with Animal Welfare Act regulations, Public Health Service policy, and *Guide for the Care and Use of Laboratory Animals* recommendations (24).

Animals were singly housed because MPXV can be transmitted by close physical contact. Environmental enrichment plans included safe and positive interaction with the animal care staff and the use of supplemental enrichment items (e.g., toys, mirrors, food-foraging devices). Additional comfort and care for the well-being of the animals, such as supplemental heat and intravenous, subcutaneous, or oral fluids, were provided as long as it was consistent with the scientific integrity of the protocol. The fruits and tasty treats, such as Gatorade, pudding, or Primadough (cookie dough-like material), provided have been well received. When animals became severely anorexic, they were tube-fed Ensure, PediaSure, or another high-calorie supplement under sedation (0.3 mg/kg of body weight of metoclopramide via intramuscular [IM] injection 15 min prior to tube feeding).

For imaging procedures, animals received ketamine sedation (10 mg/kg IM) before placement of an IV catheter in a peripheral vein (saphenous or cephalic). Animals were intubated and placed on isoflurane inhalation anesthesia (1 to 4%, to effect) in oxygen. Body temperature was maintained by supplying warm air from a Bair Hugger (3M, St. Paul, MN) directly over the animal. Additionally, a heat lamp was in place to provide extra warmth to the animal if needed.

For phlebotomy, virus injection IV, and cidofovir administration, animals were injected IM with either ketamine (10 to 25 mg/kg) or a tiletamine and zolazepam combination (3 to 6 mg/kg). Before terminal exsanguination, ketamine (25 to 40 mg/kg) or a tiletamine and zolazepam combination (6 mg/kg) was administered.

For axillary or inguinal lymph node biopsies, surgical anesthesia was provided by either an injectable combination (ketamine [10 to 25 mg/kg] + midazolam [0.1 mg/kg]) or by isoflurane by inhalation (1 to 4% in oxygen) following sedation by ketamine (10 mg/kg IM) or a tiletamine and zolazepam combination (3 to 6 mg/kg). Glycopyrrolate (0.001 to 0.005 mg/kg IM) was given after the initial sedation. For pain relief, animals were injected with a local analgesia (0.5 to 1 ml of a 0.5% solution of levobupivacaine or bupivacaine) at 20 min prior to surgery. A loss of motor reflexes and sensation to pain, as evidenced by toe-pinch reflex and lack of movement, was achieved before any procedures were performed on animals.

Cidofovir treatment. Three of six rhesus macaques were treated IV with CDV (Gilead, Foster City, CA) at 5 mg/ml/kg of body weight in Dulbecco's modified Eagle's medium (Gilead Sciences), a dose that was shown to be effective against monkeypox (17). Three animals comprised the untreated control group. CDV was administered IV on day −1 preexposure and on days 1, 3, 5, 7, 10, and 13 p.i. (17). NHPs received 25 mg/kg of probenecid (Sigma-Aldrich, St. Louis, MO) by oral gavage 1 h before CDV injection to prevent CDV-induced nephrotoxicity (17).

PET/CT imaging. At various times pre- and postinfection, NHPs were anesthetized and imaged by PET 1 h after IV injection of 1 mCi of [^{18}F]-FDG followed by CT imaging. The [^{18}F]-FDG PET images were acquired using a Focus 220 instrument (Siemens AG, Malvern, PA) with 0.9-mm-pixel resolution and 0.8-mm-slice thickness for 96 slices per bed location. The microPET Focus 220 is backed up to a small-bore clinical CT scanner (CereTom; NeuroLogica, Danvers, MA), and they share an imaging bed. CT images were acquired with settings of a 120 kV peak, 5 mA, 1.25-mm scan thickness for 190 slices with 0.49 by 0.49 mm^2 in-plane resolution.

PET and CT images were coregistered and analyzed using PMOD (PMOD Ltd., Zurich, Switzerland) and MIM software (MIM Software Inc., Cleveland, OH). Surviving ($n = 4$; 3 treated, 1 untreated) and moribund ($n = 2$) subjects were grouped for data analysis. Volumes of interest (VOIs) for BM from the manubrium and body of one thoracic vertebra were drawn on CT images and transferred to PET images. The mean standardized uptake value, SUV_{mean}, was determined as the average of all voxels in the VOI. VOIs for LN were drawn on CT images and transferred to PET images. The modified SUV threshold ($mSUV_{thr}$) was calculated by averaging the voxels in the PET images with SUVs above 50% of the maximal value inside the LN VOI (8).

Neutralizing antibody assay. Neutralizing antibody titers from MPXV-infected NHPs were measured as previously described (25).

Virus quantification by real-time PCR. Genome copies/ml in whole blood were determined by quantitative PCR as described previously (20, 26).

Hematology, flow cytometry, and blood biochemistry. Blood samples were assayed for complete blood counts with differential, and PBMCs were analyzed using Trucount tubes (BD Biosciences, San Jose, CA) as described previously (21). PBMC samples and lymphocytes isolated from LNs were surface stained with a custom antibody cocktail (BD Biosciences) for CD3, CD4, CD8, CD14, CD16, CD20, CD45, and Ki-67. Data were collected on an LSR II flow cytometer (BD Biosciences) and analyzed by FlowJo 9.3.1 software (TreeStar, Inc., Ashland, OR) or by BD FACSDiva software. Monocytes were gated first on CD45$^+$ and then on CD14$^+$. T and B cells were gated first on CD45$^+$, then further defined as CD3$^+$ CD4$^+$ T cells, CD3$^+$ CD8$^+$ T cells, and CD3$^-$ CD20$^+$ B cells.

Tissue collection, histopathology, and immunohistochemistry. Inguinal LNs were collected by excisional biopsy from the right side of healthy subjects on day −19 or −20 preexposure and from the left side on day 9 p.i., when the strongest immune response in LNs was expected based on results from a previous study (20). Necropsies were performed when animals met moribund clinical endpoint criteria or reached the study end. Tissue samples were collected from all major organs, fixed in 10% neutral buffered formalin, embedded in paraffin, sectioned to 5-μm thickness, and stained with hematoxylin and eosin (H&E). LN tissues were scored for edema, necrosis, and lymphoid depletion. Immunohistochemistry assays were performed on a Bond polymer refine detection system (Leica Microsystems, Buffalo Grove, IL) using antibodies (Biocare Medical) for CD20, CD4, CD8, and/or Ki-67. Ki-67 staining and Ki-67 costaining with CD20, CD4, or CD8 were scored as follows: 0 (not detectable), 1 (minimal), 2 (mild), 3 (moderate), or 4 (severe). Negative controls included lymphoid tissue from uninfected NHPs.

Statistical analysis. Two-way repeated-measures ANOVA was employed to explore whether the pattern of changes in [^{18}F]-FDG uptake could predict disease outcome and/or specify the effect of CDV treatment. For two-way repeated-measures ANOVA, two independent variables were used, either time (independent variable 1; the SUV in each subject was measured at 7 time points pre- and postinfection [repeated]) and survival status (independent variable 2) or time (independent variable 1) and treatment (independent variable 2). The goal was to examine the difference in SUVs (the dependent variable) either by time and survival status or by time and treatment application. ANOVA was selected because it is a more general hypothesis-testing procedure and reduces the type I error rate; therefore, it is preferred over a *t* test for such small group sizes. The analysis was also used to examine the interaction between the two independent variables that indicates that differences are not uniform across independent variables. *Post hoc* comparisons were performed using the Bonferroni test. The correlation between changes in BM SUVs and complete blood cells with differential was calculated using the Pearson product moment correlation coefficient (*r*). GraphPad Prism 6.01 (GraphPad Software, Inc., La Jolla, CA) was used for statistical analysis.

ACKNOWLEDGMENTS

This work was supported by the Battelle Memorial Institute's prime contract with the National Institute of Allergy and Infectious Diseases (NIAID) at the National Institutes of Health, under contract no. HHSN272200700016I. This work, in part, was supported by the NIAID Division of Intramural Research. Subcontractors to Battelle Memorial Institute who performed this work are J.D., S.C., D.T., C.J., and J.A.C., employees of Tunnell Government Services, Inc.; C.L. and J.S., employees of MEDRelief Staffing; and D.R.R. and R.B., employees of Charles River Laboratories.

The authors declare that they have no conflict of interest.

We thank Jennifer Hufton, Cindy Allan, Erika Zommer, Isis Alexander, Nick Oberlander, and Bernardo Rosa for their contributions to these studies. We thank Laura Bollinger and Jiro Wada for technical writing services and figure preparation, respectively.

REFERENCES

1. Fenner F. 1980. The global eradication of smallpox. Med J Aust 1:455–455.
2. Food and Drug Administration, Department of Health and Human Services. 2014. Approval of new drugs when human efficacy studies are not ethical or feasible, p 174–177. Code of Federal Regulations, Title 21, part 314, subpart 1. Government Printing Office, Washington, DC.
3. Chapman JL, Nichols DK, Martinez MJ, Raymond JW. 2010. Animal models of orthopoxvirus infection. Vet Pathol 47:852–870. https://doi.org/10.1177/0300985810378649.
4. Biomarkers Definitions Working Group. 2001. Biomarkers and surrogate endpoints: preferred definitions and conceptual framework. Clin Pharmacol Ther 69:89–95. https://doi.org/10.1067/mcp.2001.113989.
5. Jordan R, Hruby D. 2006. Smallpox antiviral drug development: satisfying the animal efficacy rule. Expert Rev Anti Infect Ther 4:277–289. https://doi.org/10.1586/14787210.4.2.277.
6. Parker S, Chen NG, Foster S, Hartzler H, Hembrador E, Hruby D, Jordan R, Lanier R, Painter G, Painter W, Sagartz JE, Schriewer J, Mark Buller R. 2012. Evaluation of disease and viral biomarkers as triggers for therapeutic intervention in respiratory mousepox—an animal model of smallpox. Antiviral Res 94:44–53. https://doi.org/10.1016/j.antiviral.2012.02.005.
7. Parker S, Schriewer J, Oberle C, Robertson A, Lanier R, Painter G, Buller RM. 2008. Using biomarkers to stage disease progression in a lethal mousepox model treated with CMX001. Antivir Ther 13:863–873.
8. Chefer S, Reba R, Leyson C, Seidel J, Johnson R, Blaney J, Jahrling P, Dyall J. 2014. The effect of volume of interest definition on quantification of lymph node immune response to a monkeypox virus infection assessed by (18)F-FDG-PET. EJNMMI Res 4:49. https://doi.org/10.1186/s13550-014-0049-z.
9. Dyall J, Johnson RF, Chen DY, Huzella L, Ragland DR, Mollura DJ, Byrum R, Reba RC, Jennings G, Jahrling PB, Blaney JE, Paragas J. 2011. Evaluation of monkeypox disease progression by molecular imaging. J Infect Dis 204:1902–1911. https://doi.org/10.1093/infdis/jir663.
10. Mollura DJ, Asnis DS, Crupi RS, Conetta R, Feigin DS, Bray M, Taubenberger JK, Bluemke DA. 2009. Imaging findings in a fatal case of pandemic swine-origin influenza A (H1N1). AJR Am J Roentgenol 193:1500–1503. https://doi.org/10.2214/AJR.09.3365.
11. Scharko AM, Perlman SB, Hinds PW, Hanson JM, Uno H, Pauza CD. 1996. Whole body positron emission tomography imaging of simian immunodeficiency virus-infected rhesus macaques. Proc Natl Acad Sci U S A 93:6425–6430. https://doi.org/10.1073/pnas.93.13.6425.
12. Scharko AM, Perlman SB, Pyzalski RW, Graziano FM, Sosman J, Pauza CD. 2003. Whole-body positron emission tomography in patients with HIV-1 infection. Lancet 362:959–961. https://doi.org/10.1016/S0140-6736(03)14366-8.
13. Via LE, Schimel D, Weiner DM, Dartois V, Dayao E, Cai Y, Yoon YS, Dreher MR, Kastenmayer RJ, Laymon CM, Carny JE, Flynn JL, Herscovitch P, Barry CE, III. 2012. Infection dynamics and response to chemotherapy in a rabbit model of tuberculosis using [^{18}F]2-fluorodeoxy-D-glucose positron emission tomography and computed tomography. Antimicrob Agents Chemother 56:4391–4402. https://doi.org/10.1128/AAC.00531-12.
14. Wallace M, Pyzalski R, Horejsh D, Brown C, Djavani M, Lu Y, Hanson JM, Mitchen JL, Perlman SB, Pauza CD. 2000. Whole body positron emission tomography imaging of activated lymphoid tissues during acute simian-human immunodeficiency virus 89.6PD infection in rhesus macaques. Virology 274:255–261. https://doi.org/10.1006/viro.2000.0479.
15. Zaitseva M, Kapnick S, Golding H. 2012. Measurements of vaccinia virus dissemination using whole body imaging: approaches for predicting of lethality in challenge models and testing of vaccines and antiviral treatments. Methods Mol Biol 890:161–176. https://doi.org/10.1007/978-1-61779-876-4_10.
16. Zaitseva M, Kapnick SM, Scott J, King LR, Manischewitz J, Sirota L, Kodihalli S, Golding H. 2009. Application of bioluminescence imaging to the prediction of lethality in vaccinia virus-infected mice. J Virol 83:10437–10447. https://doi.org/10.1128/JVI.01296-09.

17. Stittelaar KJ, Neyts J, Naesens L, van Amerongen G, van Lavieren RF, Holy A, De Clercq E, Niesters HG, Fries E, Maas C, Mulder PG, van der Zeijst BA, Osterhaus AD. 2006. Antiviral treatment is more effective than smallpox vaccination upon lethal monkeypox virus infection. Nature 439:745–748. https://doi.org/10.1038/nature04295.
18. Murata Y, Kubota K, Yukihiro M, Ito K, Watanabe H, Shibuya H. 2006. Correlations between 18F-FDG uptake by bone marrow and hematological parameters: measurements by PET/CT. Nucl Med Biol 33:999–1004. https://doi.org/10.1016/j.nucmedbio.2006.09.005.
19. Shreve PD, Anzai Y, Wahl RL. 1999. Pitfalls in oncologic diagnosis with FDG PET imaging: physiologic and benign variants. Radiographics 19: 61–77. https://doi.org/10.1148/radiographics.19.1.g99ja0761.
20. Johnson RF, Dyall J, Ragland DR, Huzella L, Byrum R, Jett C, St. Claire M, Smith AL, Paragas J, Blaney JE, Jahrling PB. 2011. Comparative analysis of monkeypox virus infection of cynomolgus macaques by the intravenous or intrabronchial inoculation route. J Virol 85:2112–2125. https://doi.org/10.1128/JVI.01931-10.
21. Song H, Janosko K, Johnson RF, Qin J, Josleyn N, Jett C, Byrum R, St. Claire M, Dyall J, Blaney JE, Jennings G, Jahrling PB. 2013. Poxvirus antigen staining of immune cells as a biomarker to predict disease outcome in monkeypox and cowpox virus infection in non-human primates. PLoS One 8:e60533. https://doi.org/10.1371/journal.pone.0060533.
22. Lederman ER, Reynolds MG, Karem K, Braden Z, Learned-Orozco LA, Wassa-Wassa D, Moundeli O, Hughes C, Harvey J, Regnery R, Mombouli JV, Damon IK. 2007. Prevalence of antibodies against orthopoxviruses among residents of Likouala region, Republic of Congo: evidence for monkeypox virus exposure. Am J Trop Med Hyg 77:1150–1156.
23. Chefer S, Thomasson D, Seidel J, Reba RC, Bohannon JK, Lackemeyer MG, Bartos C, Sayre PJ, Bollinger L, Hensley LE, Jahrling PB, Johnson RF. 2015. Modeling [18F]-FDG lymphoid tissue kinetics to characterize nonhuman primate immune response to Middle East respiratory syndrome-coronavirus aerosol challenge. EJNMMI Res 5:65. https://doi.org/10.1186/s13550-015-0143-x.
24. National Research Council. 2011. Guide for the care and use of laboratory animals, 8th ed. National Academies Press, Washington, DC.
25. Earl PL, Americo JL, Moss B. 2003. Development and use of a vaccinia virus neutralization assay based on flow cytometric detection of green fluorescent protein. J Virol 77:10684–10688. https://doi.org/10.1128/JVI.77.19.10684-10688.2003.
26. Sofi Ibrahim M, Kulesh DA, Saleh SS, Damon IK, Esposito JJ, Schmaljohn AL, Jahrling PB. 2003. Real-time PCR assay to detect smallpox virus. J Clin Microbiol 41:3835–3839. https://doi.org/10.1128/JCM.41.8.3835-3839.2003.